Journal of
Marine Science and Engineering

MDPI

Article

Acoustic Transmission Loss of a Cylindrical Silencer Filled with Multilayer Poroelastic Materials Based on Mode-Matching Method

Haesang Yang [1] and Woojae Seong [2,*]

[1] Department of Artificial Intelligence and Robotics, Sejong University, Seoul 05006, Republic of Korea; haesang.yang@sejong.ac.kr
[2] Department of Naval Architecture and Ocean Engineering/Research Institute of Marine Systems Engineering, Seoul National University, Seoul 08826, Republic of Korea
* Correspondence: wseong@snu.ac.kr; Tel.: +82-2-880-8359

Abstract: The efficacy of silencers in reducing piping noise is contingent upon the specific installation and operating environment. Among the various forms of silencers, the acoustic characteristics of dissipative silencers with sound-absorbing materials attached internally exist in an area that is difficult to explain by existing theories. This is dependent upon the specific type and placement of the attached sound-absorbing materials. This paper presents a methodology for calculating the acoustic transmission loss (TL) of a cylindrical silencer filled with a multilayer poroelastic material, employing the mode-matching method. To describe the numerical process of treating waves propagating within a poroelastic material and determine the modes in accordance with the boundary conditions necessary for analyzing the acoustic performance of the silencer, the Biot model and the Johnson–Champoux–Allard–Lafarge model were employed. The obtained modes were utilized to calculate the acoustic TL of silencers filled with single, double, and triple layers of poroelastic materials. In particular, the results obtained for the single layer were validated by comparing them with the results of a finite element analysis, and the results obtained for multiple layers with the same material were validated by comparing them with the equivalent single-layer results. Moreover, the results of the numerical calculations of the acoustic TLs of the silencer for three distinct types of poroelastic materials, including those with varying degrees of frame rigidity or softness, were compared, and the acoustic characteristics were analyzed in relation to the intrinsic properties of the materials and their arrangement. It is anticipated that the methodology presented in this paper will facilitate the design of silencers using poroelastic materials in accordance with the specific requirements of users or designers by allowing for a comprehensive consideration of the thickness of layers and the arrangement of materials.

Keywords: Biot theory; Johnson–Champoux–Allard–Lafarge model; mode-matching; silencer; poroelastic material; transmission loss

Citation: Yang, H.; Seong, W. Acoustic Transmission Loss of a Cylindrical Silencer Filled with Multilayer Poroelastic Materials Based on Mode-Matching Method. *J. Mar. Sci. Eng.* **2024**, *12*, 2109. https://doi.org/10.3390/jmse12112109

Academic Editors: Kostas Belibassakis, Claudio Testa and Giovanni Bernardini

Received: 18 October 2024
Revised: 18 November 2024
Accepted: 18 November 2024
Published: 20 November 2024

1. Introduction

The marine and offshore industries are prone to the occurrence of unnecessary or unintended noise and vibration. In particular, noise and vibration from ships and offshore structures represent a significant challenge, with the potential to impact the safety and well-being of crew, passengers, and related personnel, as well as the integrity of marine ecosystems [1–3]. Consequently, a range of methodologies have been proposed and investigated with the aim of reducing such noise and vibration [4,5].

Silencers are often used to reduce noise in a variety of marine or offshore applications, including shipbuilding, ducting and pipes, heating, ventilation, air conditioning (HVAC), and more. Silencers are broadly categorized into reflective and dissipative (or absorptive) silencers. In general, reflective silencers perform better in the low-frequency band, while

dissipative silencers perform better in the mid-to-high-frequency band [6,7]. To improve the performance of a silencer, it is useful to use a dissipative silencer, which has a better performance-to-size ratio, rather than increasing the size of the reflective silencer itself.

The principle of dissipative silencers is that as sound waves propagate, the sound energy is converted into heat by the sound-absorbing material attached to the inside of the silencer, reducing the sound energy after passing through the silencer, thus reducing noise [8]. Many studies have been conducted to evaluate the performance of these dissipative silencers. Craggs [9] studied the acoustic behavior of a simple expanding chamber lined with sound-absorbing material using the finite element method (FEM) and found that the transmission loss (TL) varied with the sound-absorbing material and that the maximum TL frequency changed with increasing the sound-absorbing material thickness. Peat [10] developed a transfer matrix method for bulk-reactive dissipative silencers to provide a more convenient way to calculate acoustic performance. Xu et al. [7] compared and analyzed the theoretical and numerical results of the influence of sound-absorbing material properties, such as material thickness and flow resistance, on the acoustic performance of a simple expanded dissipative silencer.

Here are some recent research trends that are relevant. First, Hergli and Mosbahi [11] numerically calculated the TLs of various shapes of dissipative silencers based on FEM. Benchea et al. [12] focused on an acoustic study of different materials lining three commercial silencers of the same geometry and size. Jokandan et al. [13] investigated the combined and independent effects of baffles and expansion tubes, the reactive elements at the inlet and outlet of a simple expansion silencer, on the acoustic performance and pressure loss of a simple expansion silencer and concluded that the best acoustic performance at mid-frequencies was achieved by using a combination of baffles and expansion tubes. Even if the fluid in the pipe is water, there are various types of silencers, and studies have been published to analyze the acoustic performance of perforated pipe silencers with computational fluid dynamics approaches [14] to analyze Helmholtz resonator-type silencers with time–domain finite volume methods [15], or to reduce low-frequency noise by creating a metamaterial effect by periodically mounting Helmholtz resonators [16].

In addition to the above, the type of sound-absorbing material attached to the inside of the dissipative silencer may need to be different depending on the piping situation and operating environment. Common sound-absorbing materials can be divided into two broad categories based on their physical properties. First, there are fiber-based materials such as glass wool. The model used to predict the sound absorption performance of these materials is the Delany and Bazley model [17], which predicts the characteristic impedance of a sound-absorbing material from its flow resistivity. As a specific application, Selamet et al. [18] used the characteristic impedance and propagation constant obtained from the flow resistivity to find the acoustic attenuation performance of perforated dissipative circular expansion chambers with inlet/outlet extensions. This model for predicting characteristic impedance from flow resistivity performs quite well in predicting the sound absorption performance of fiber-based materials.

Another type of sound-absorbing material is a foam-like material. The aforementioned prediction of characteristic impedance from flow resistivity is not suitable for predicting the sound absorption performance of foam-like materials, where the motion of the skeleton affects the sound attenuation. This is where the Biot model comes in handy. Biot [19,20] presented a theory of wave propagation that considers the interaction of fluids and solids in a fully saturated porous medium. Among the many coefficients required by Biot's theory, the Johnson–Champoux–Allard–Lafarge (JCAL) model is well known, as it allows for the effective density and effective bulk modulus to be expressed in terms of measurable variables [21]. Nennig et al. [22] presented a mode-matching method to find the TL of a cylindrical duct filled with a single poroelastic material using the Biot and JCAL models.

The effects of multiple layers of sound-absorbing materials inside a silencer on acoustic performance have also been reported. Selamet et al. [23] published an analytical analysis of the acoustic performance of a dissipative expansion chamber filled with two layers of

fibrous material, while Veerababu and Venkatesham [24] investigated the TL of a circular dissipative chamber filled with multiple layers of fibrous material using a tailored Green's function. However, these studies were for fibrous materials, and the acoustic performance of silencers with multiple layers of foam-like sound-absorbing materials has not been studied. Especially for pipe silencers used in situations where strong external pressure is applied, it is necessary to use poroelastic materials such as foam with strong skeletal rigidity, but it is difficult to manufacture and attach large sound-absorbing materials at once, so silencers are manufactured and operated with sound-absorbing materials composed of multiple layers. Therefore, it is essential to predict the acoustic performance of dissipative silencers with multilayer poroelastic materials.

This study extends the work of [22], which only considered a single layer of poroelastic material, to propose a mode-matching method for predicting the acoustic performance of a silencer considering multilayer poroelastic materials. Prior to this study, several studies have investigated the acoustic performance of ducts containing single-layer poroelastic material or multilayer sound absorbers made of fiber materials based on the mode-matching method. However, no study has investigated the acoustic performance of a silencer considering multilayer poroelastic materials as in this study. In this study, Biot's theory and the JCAL model were used to obtain the necessary coupled equations for the analysis of a cylindrical silencer filled with multiple layers of poroelastic materials, and numerical tests showed that a fairly accurate TL could be obtained using only the first 12 modes in a silencer filled with two layers of poroelastic materials. The results of the mode-matching method presented in this study were validated by comparing them with the results of calculations using COMSOL Multiphysics® 6.2 software.

The rest of this paper is organized as follows. In Section 2, the problem statement and formulation are described. The root-finding and mode-matching methods are explained in Section 3. In Section 4, the results are presented and discussed. This study is concluded in Section 5.

2. Problem Statement

2.1. Governing Equations

Consider a cylindrical silencer with N layers of poroelastic material arranged in a cylindrical duct of length L, as shown in Figure 1. At the center is air with an average flow rate of zero. From the center, the distance to the first poroelastic material is called r_1; the distance to the second poroelastic material is called r_2; the distance to N-th poroelastic material is called r_N, and the distance to the wall of the silencer is called r_{N+1}.

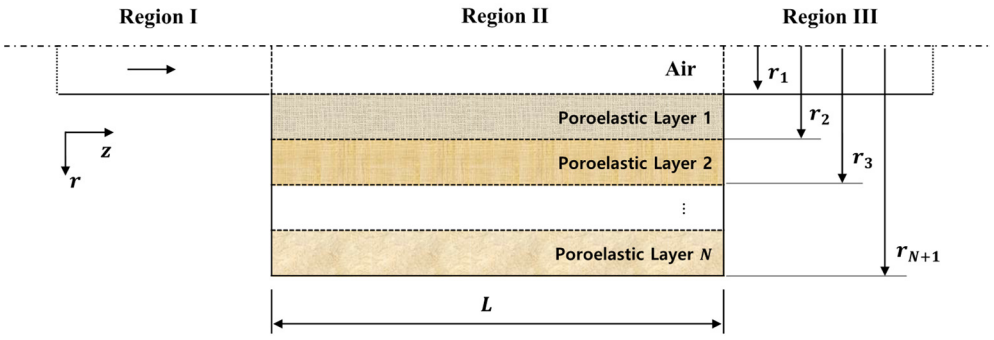

Figure 1. Schematic diagram of a cylindrical silencer with multilayered poroelastic material.

In the center of the airflow ($0 < r < r_1$), let the speed of sound in the air be c_0, the wavenumber be k_0, the angular frequency be ω, and the z-direction wavenumber be k_z. The sound pressure and displacement satisfy the wave Equation (1) and Euler's Equation (2).

$$\nabla^2 p = \frac{1}{c_0^2}\frac{\partial^2 p}{\partial t^2}, \tag{1}$$

$$\rho_0 \frac{\partial^2 \mathbf{w}}{\partial t^2} = -\nabla p. \tag{2}$$

Substituting the displacement potential ϕ_0 satisfying $\mathbf{w} = \nabla\phi_0$ into (2), the acoustic pressure is expressed as follows:

$$p = \rho_0 c_0^2 k_0^2 \phi_0. \tag{3}$$

Solving (1) through (3), the following expressions can be obtained:

$$\phi_0 = A_0 J_m(k_{0r} r)\cos m\theta \; e^{j(k_z z - \omega t)}, \tag{4}$$

$$k_{0r}^2 = k_0^2 - k_z^2, \tag{5}$$

where k_{0r} is the r-directional wavenumber of the air. For convenience, the term $e^{j(k_z z - \omega t)}$ in the following expressions will be omitted.

Inside a poroelastic medium ($r_n < r < r_{n+1}, \quad n = 1, 2, \ldots, N$), there are compressional waves propagating through repeated expansion and contraction and shear waves propagating through rotational motion. According to the Biot model, sound propagation in the poroelastic medium is affected by the interaction of solids and fluids and can be modeled as the sum of two compressional waves and one shear wave. Through Helmholtz decomposition, the displacement **u** of the solid and the average displacement **U** of the fluid can be expressed in terms of the displacement potential as follows:

$$\mathbf{u} = \nabla\phi_1 + \nabla\phi_2 + \nabla \times \psi, \tag{6}$$

$$\mathbf{U} = \mu_1 \nabla\phi_1 + \mu_2 \nabla\phi_2 + \mu_3 \nabla \times \psi, \tag{7}$$

where μ_1, μ_2 are the ratios of amplitudes between the compressional waves in the fluid and solid, and μ_3 is the ratio of amplitudes between the shear waves. The exact expressions for μ_1, μ_2, and μ_3 will be explained at the end of this section.

Furthermore, in (6) and (7), ϕ_1 and ϕ_2 denote the displacement potentials of the two compressional waves, and ψ denotes the displacement potential of the shear wave, and each displacement potential is expressed as follows [25].

$$\phi_{1,n} = [A_{1,n} J_m(k_{1r,n} r) + B_{1,n} Y_m(k_{1r,n} r)]\cos m\theta, \tag{8}$$

$$\phi_{2,n} = [A_{2,n} J_m(k_{2r,n} r) + B_{2,n} Y_m(k_{2r,n} r)]\cos m\theta, \tag{9}$$

$$\psi_{r,n} = [A_{3,n} J_{m+1}(k_{3r,n} r) + B_{3,n} Y_{m+1}(k_{3r,n} r)]\sin m\theta, \tag{10}$$

$$\psi_{\theta,n} = -[A_{3,n} J_{m+1}(k_{3r,n} r) + B_{3,n} Y_{m+1}(k_{3r,n} r)]\cos m\theta, \tag{11}$$

$$\psi_{z,n} = \left[A'_{3,n} J_{m+1}(k_{3r,n} r) + B'_{3,n} Y_{m+1}(k_{3r,n} r)\right]\sin m\theta, \tag{12}$$

$$k_{ir,n}^2 = k_{i,n}^2 - k_z^2, \qquad i = 1, 2, 3. \tag{13}$$

Considering that ψ_r, ψ_θ, and ψ_z denote the components of ψ in the cylindrical coordinate system and given that the Helmholtz equation in the cylindrical coordinate system has the form of a Bessel equation, it is natural that the displacement potentials in (8) to (12) have the form of Bessel functions. Only the $m = 0$ mode will be used, which is axisymmetric and does not depend on the θ-direction. The subscript n refers to the n-th layer of poroelastic material inside the silencer. Equation (13) is virtually the same expression as (5).

For solids and fluids, the stress–strain relationships are as follows, respectively:

$$\sigma_{ij}^s = [(P - 2S)u_{i,i} + QU_{i,i}]\delta_{ij} + S\left(\frac{\partial u_i}{\partial x_j} + \frac{\partial u_j}{\partial x_i}\right), \tag{14}$$

$$\sigma_{ij}^f = [Qu_{i,i} + RU_{i,i}]\delta_{ij}. \tag{15}$$

where $u_{i,i} = \nabla \cdot \mathbf{u}$, and $U_{i,i} = \nabla \cdot \mathbf{U}$.

The total stress and pore pressures are expressed as follows, respectively:

$$\sigma_{ij}^{t} = \sigma_{ij}^{s} + \sigma_{ij}^{f}, \tag{16}$$

$$p_p = -\frac{1}{3\phi} tr\left(\sigma^f\right). \tag{17}$$

P, Q, R, and S in (14) and (15) are coefficients that can be deduced from Biot's Gedanken experiment. S is the complex shear modulus of the skeleton of the poroelastic material. According to [21], P, Q, and R are expressed as follows, if the material forming the skeleton is incompressible:

$$P = \frac{4}{3}S + K_b + \frac{(1-\phi)^2}{\phi}K_f, \tag{18}$$

$$Q = K_f(1-\phi), \tag{19}$$

$$R = \phi K_f, \tag{20}$$

where the bulk modulus of the frame is the relationship between the Lamé constant and the Poisson's ratio ν, which is defined as

$$K_b = \frac{2S(\nu+1)}{3(1-2\nu)}. \tag{21}$$

Since the air inside the poroelastic material interacts with the frame, the bulk modulus and density of the air change complexly with the frequency. In this study, the JCAL model is applied to represent K_f and ρ_f [21] as follows:

$$\rho_f = \alpha_\infty \rho_0 \left[1 + \frac{j\sigma\phi}{\omega\rho_{0\,\infty}}\sqrt{1 - j\frac{4\alpha_\infty^2\eta\rho_0\omega}{\sigma^2\Lambda^2\phi^2}}\right], \tag{22}$$

$$K_f = \frac{\gamma P_0}{\gamma - (\gamma-1)/\left[1 + j\frac{\phi\kappa}{k_0' C_p\rho_0\omega}\sqrt{1 - j\frac{4k_0'^2 C_p\rho_0\omega}{\kappa\Lambda'^2\phi^2}}\right]}, \tag{23}$$

where α_∞ is the tortuosity; ϕ is the porosity; σ is the flow resistivity; ρ_0 is the density of the air; η is the viscosity of the air; κ is the thermal conductivity of the air; C_p is the static pressure specific heat; Λ is the viscous characteristic length; Λ' is the thermal characteristic length; γ is the specific heat ratio, and P_0 is the atmospheric pressure. k_0' is the static thermal conductivity and is defined in the simplified Lafarge model as follows [21]:

$$q_0' = \frac{\phi\Lambda'^2}{8}. \tag{24}$$

In Biot theory, there are two compressional waves (subscripts 1 and 2) and one shear wave (subscript 3) in a poroelastic medium, each with the following wavenumbers:

$$k_1^2 = \frac{\omega^2}{2(PR-Q^2)}\left[P\rho_{22} + R\rho_{11} - 2Q\rho_{12} + \sqrt{\Delta}\right], \tag{25}$$

$$k_2^2 = \frac{\omega^2}{2(PR-Q^2)}\left[P\rho_{22} + R\rho_{11} - 2Q\rho_{12} - \sqrt{\Delta}\right], \tag{26}$$

$$k_3^2 = \frac{\omega^2}{S}\left(\frac{\rho_{11}\rho_{22} - \rho_{12}^2}{\rho_{22}}\right),\ \psi_{r,n} = [A_{3,n}J_{m+1}(k_{3r,n}r) + B_{3,n}Y_{m+1}(k_{3r,n}r)]\sin m\theta, \tag{27}$$

$$\Delta = [P\rho_{22} + R\rho_{11} - 2Q\rho_{12}]^2 - 4\Big(PR - Q^2\Big)\Big(\rho_{11}\rho_{12} - \rho_{12}^2\Big), \tag{28}$$

$$\rho_{22} = \rho_f \phi, \tag{29}$$

$$\rho_{12} = \Big(\rho_0 - \rho_f\Big)\phi, \tag{30}$$

$$\rho_{11} = \rho_1 - \rho_{12}, \tag{31}$$

$$\rho_1 = (1-\phi)\rho_s, \tag{32}$$

where ρ_s is the density of the material that makes up the frame, and ρ_1 is the apparent density of the frame considering the porosity.

Using the expressions described so far, μ_1, μ_2, and μ_3 in (7) can be found as follows:

$$\mu_1 = \frac{Pk_1^2 - \omega^2\rho_{11}}{\omega^2\rho_{12} - Qk_1^2}, \tag{33}$$

$$\mu_2 = \frac{Pk_2^2 - \omega^2\rho_{11}}{\omega^2\rho_{12} - Qk_2^2}, \tag{34}$$

$$\mu_3 = -\frac{\rho_{12}}{\rho_{22}}. \tag{35}$$

2.2. Boundary Conditions

The boundary conditions between the air and the poroelastic material ($r = r_1$) are as follows [22]:

$$\sigma_1^t \mathbf{n} = -p\mathbf{n}, \tag{36}$$

$$\phi_1 \mathbf{U}_1 \cdot \mathbf{n} + (1-\phi_1)\mathbf{u}_1 \cdot \mathbf{n} = \mathbf{w} \cdot \mathbf{n}, \tag{37}$$

$$p_{p,1} = p, \tag{38}$$

where the subscript 1 is the poroelastic material of the first layer, and $\mathbf{n}$ is the normal vector. Equation (36) describes the equilibrium of stress and pressure, (37) represents the continuity of the mass flux, and (38) represents the continuity of pressure.

At the interface between two different poroelastic materials, the boundary condition is as follows [26]:

$$\sigma_n^t \mathbf{n} = \sigma_{n+1}^t \mathbf{n}, \tag{39}$$

$$\mathbf{u}_n = \mathbf{u}_{n+1}, \tag{40}$$

$$\phi_n(\mathbf{U}_n \cdot \mathbf{n} - \mathbf{u}_n \cdot \mathbf{n}) = \phi_{n+1}(\mathbf{U}_{n+1} \cdot \mathbf{n} - \mathbf{u}_{n+1} \cdot \mathbf{n}), \tag{41}$$

$$p_{p,n} = p_{p,n+1}, \tag{42}$$

where (39) describes the continuity of stress; (40) describes the continuity of the solid displacement; (41) represents the continuity of the mass flux, and (42) represents the continuity of the pore pressure.

Using the expressions of Biot's theory described in Section 2.1, the boundary conditions of (36) through (42) are expressed in a total of $6N + 1$ equations, where N is the number of the poroelastic layers. These boundary conditions are expressed in matrix form as follows:

$$\mathbf{X} = \begin{pmatrix} A_{1,1}, B_{1,1}, A_{2,1}, B_{2,1}, A_{3,1}, B_{3,1}, A_{1,2}, B_{1,2}, A_{2,2}, B_{2,2}, \ldots, \\ A_{1,N}, B_{1,N}, A_{2,N}, B_{2,N}, A_{3,N}, B_{3,N}, A_0 \end{pmatrix}^T, \tag{43}$$

$$\mathbf{C}(k_Z)\mathbf{X} = 0, \tag{44}$$

where $\mathbf{C}$ is a square matrix of size $6N + 1$, and the components of the matrix are specified in Appendix A.

3. Root-Finding and Mode-Matching

3.1. Root-Finding

For (44) to have a nontrivial solution, it is necessary to find a k_z that satisfies $\det(\mathbf{C}(k_z)) = 0$. Numerically, it is sufficient to use the Newton–Raphson method, which is often used to find roots, but in this study, the Muller's method is used. Since matrices with very large condition numbers are dealt with, it is needed to be careful with rounding errors. As the number of poroelastic layers increases, these errors become more significant. Minimizing the rounding error is essential to using the mode-matching method.

Numerical methods for finding roots, such as the Newton–Raphson method, the Secant method, and the Muller's method, all require an initial value, and since it is hard to predict which roots will be found based on the initial value, it is important to iterate over enough initial values to ensure that no roots are missed. In reference [22], Nennig et al. propose a method to find roots without missing roots using the argument principle. However, this method has the disadvantage of taking longer than Newton–Raphson method, and large rounding errors can give incorrect results, so it is not used in this study.

3.2. Mode-Matching

The physical meaning of the mode-matching method is that it is very useful for formulating boundary value problems for structures composed of two or more separate regions. Since this method is based on matching the fields at the boundaries of different regions, it is well-suited for analyzing boundary value problems for acoustic waves. This mode-matching method has been widely used to analyze sound transmission problems in waveguides, especially when dealing with discontinuities and obstacles in the waveguide, such as irregular geometry of the pipe or silencers.

The most employed techniques for forecasting the acoustic performance of a silencer encompass the analytical mode-matching approach [18,22,23] and numerical methods [27–29], including the FEM and the boundary element method. The application of the analytic mode-matching method is constrained to relatively simple configurations, such as circular or rectangular silencers. The numerical methods are capable of handling complex configurations; however, they are exceedingly time-consuming when the dimensions of the silencer are considerable or when the calculation frequency is very high. Considering the constraints imposed by the mode-matching method and the numerical method, the numerical mode-matching methods that integrate the numerical and mode-matching methods have been developed [30–34]. Moreover, mesh-free methods [35,36], which obviate the need for mesh generation inherent to classical numerical techniques, are also being explored. However, as the objective of this study is to examine the effect of multilayer poroelastic materials on the acoustic performance of silencers, it is confined to the analytical mode-matching method and not numerical methods.

This research has basically followed the notation of reference [22]. In the air layer within the silencer, the pressure p can be approximated using modes as follows:

$$p^i = \sum_{m=1}^{K} \left(e^{jk_{z,m}^{i,+}z} \Phi_{p,m}^{i,+}(r) A_m^{i,+} + e^{jk_{z,m}^{i,-}z} \Phi_{p,m}^{i,-}(r) A_m^{i,-} \right), \tag{45}$$

where $i =$ I, II, III (see Figure 1). K is the number of modes used, and $k_{z,m}^{i,+}$ is the element with the m-th smallest imaginary part among the k_z (K modes) found in the i region. The + and − signs above are the directions of wave propagation. The process of finding $k_{z,m}^{i,+}$ in the $i =$ II region filled with the poroelastic material has been described so far. The

modes in the air passage $i = \mathrm{I}$ or III regions are obtained by finding k_{0r} through the wall condition $J_1(k_{0r}r_1) = 0$ and then using (5) and (46):

$$k_z^{i,\pm} = \pm\sqrt{k_0^2 - \left(k_{0r}^i\right)^2}. \tag{46}$$

In (45), $\Phi_{p,m}^{i,\pm}$ is the m-th eigenfunction of pressure and is equal to (3). $A_m^{i,\pm}$ is the coefficient preceding the m-th eigenfunction.

When $z = 0$ (the boundary between $i = I$ and $i = II$), (45) can be expressed simply as follows:

$$p^I = \mathbf{\Phi}_p^{I,+}\mathbf{A}^{I,+} + \mathbf{\Phi}_p^{I,-}\mathbf{A}^{I,-}, \tag{47}$$

$$p^{II} = \mathbf{\Phi}_p^{II,+}\mathbf{A}^{II,+} + \mathbf{\Phi}_p^{II,-}\mathbf{A}^{II,-}. \tag{48}$$

where $\mathbf{\Phi}_p^{i,\pm}$ and $\mathbf{A}^{i,\pm}$ are vectors of length K with each mode as an element and defined as follows:

$$\mathbf{\Phi}_p^{i,\pm} = \left[\Phi_{p,1}^{i,\pm}, \Phi_{p,2}^{i,\pm}, \ldots, \Phi_{p,K}^{i,\pm}\right], \tag{49}$$

$$\mathbf{A}^{i,\pm} = \left[A_1^{i,\pm}, A_2^{i,\pm}, \ldots, A_K^{i,\pm}\right]^T. \tag{50}$$

When $z = L$ (the boundary between $i = II$ and $i = III$), (45) is represented as follows:

$$p^{II} = \mathbf{\Phi}_p^{II,+}\mathbf{E}^{II,+}\mathbf{A}^{II,+} + \mathbf{\Phi}_p^{II,-}\mathbf{E}^{II,-}\mathbf{A}^{II,-}, \tag{51}$$

$$p^{III} = \mathbf{\Phi}_p^{III,+}\mathbf{E}^{III,+}\mathbf{A}^{III,+} + \mathbf{\Phi}_p^{III,-}\mathbf{E}^{III,-}\mathbf{A}^{III,-}, \tag{52}$$

$$\mathbf{E}^{i,+} = diag\left(e^{jk_{z,1}^{i,+}L}, \ldots, e^{jk_{z,K}^{i,+}L}\right), \tag{53}$$

$$\mathbf{E}^{i,-} = diag\left(e^{jk_{z,1}^{i,-}L}, \ldots, e^{jk_{z,K}^{i,-}L}\right). \tag{54}$$

Since the difference between the pressure expressions at the inlets ((47) and (48)) and outlets ((51) and (52)) is simply a matter of multiplying the diagonal matrix $\mathbf{E}^{i,\pm}$ by the phase difference caused by the wave traveling over length L, the $z = 0$ ($i = \mathrm{I}$, II) case is described here, and the $z = L$ case does not repeat the same process.

Similarly to (47), the displacement $\mathbf{w}$ of the air at the inlet and the fluid displacement $\mathbf{U}$ and solid displacement $\mathbf{u}$ in the poroelastic material can be expressed in the following form:

$$w_z^i = \Phi_{w_z}^{i,+}\mathbf{A}^{i,+} + \Phi_{w_z}^{i,-}\mathbf{A}^{i,-}, \tag{55}$$

$$U_{z,n}^i = \Phi_{U_{z,n}}^{i,+}\mathbf{A}^{i,+} + \Phi_{U_{z,n}}^{i,-}\mathbf{A}^{i,-}, \tag{56}$$

$$u_{z,n}^i = \Phi_{u_{z,n}}^{i,+}\mathbf{A}^{i,+} + \Phi_{u_{z,n}}^{i,-}\mathbf{A}^{i,-}, \tag{57}$$

$$u_{r,n}^i = \Phi_{u_{r,n}}^{i,+}\mathbf{A}^{i,+} + \Phi_{u_{r,n}}^{i,-}\mathbf{A}^{i,-}. \tag{58}$$

Again, like (49), the following definition is used,

$$\mathbf{\Phi}_{w_z}^{i,\pm} = \left[\Phi_{w_z,1}^{i,\pm}, \Phi_{w_z,2}^{i,\pm}, \ldots, \Phi_{w_Z,K}^{i,\pm}\right], \tag{59}$$

$$\mathbf{\Phi}_{U_z}^{i,\pm} = \left[\Phi_{U_z,1}^{i,\pm}, \Phi_{U_z,2}^{i,\pm}, \ldots, \Phi_{U_Z,K}^{i,\pm}\right], \tag{60}$$

$$\mathbf{\Phi}_{u_z}^{i,\pm} = \left[\Phi_{u_z,1}^{i,\pm}, \Phi_{u_z,2}^{i,\pm}, \ldots, \Phi_{u_Z,K}^{i,\pm}\right], \tag{61}$$

$$\mathbf{\Phi}_{u_r}^{i,\pm} = \left[\Phi_{u_r,1}^{i,\pm}, \Phi_{u_r,2}^{i,\pm}, \ldots, \Phi_{u_r,K}^{i,\pm}\right]. \tag{62}$$

The boundary conditions (for pressure p and displacements w_z, $U_{z,n}$, $u_{z,n}$, $u_{r,n}$) between Region I and Region II at $z = 0$ are as follows:

$$p^I = p^{II}, \tag{63}$$

$$w_z^I = w_z^{II}, \tag{64}$$

$$U_{z,n}^{II} = 0, \tag{65}$$

$$u_{z,n}^{II} = 0, \tag{66}$$

$$u_{r,n}^{II} = 0. \tag{67}$$

To satisfy all the boundary conditions in (63) through (67), infinite modes are required, but since only K modes are considered, it is customary to write the above boundary conditions in integral form to solve the equations. The integral form of the boundary conditions is as follows:

$$\int_0^{r_1} p^I \overline{\Psi}_{p,m} r dr = \int_0^{r_1} p^{II} \overline{\Psi}_{p,m} r dr, \tag{68}$$

$$\int_0^{r_1} w_z^I \overline{\Psi}_{w_z,m} r dr = \int_0^{r_1} w_z^{II} \overline{\Psi}_{w_z,m} r dr, \tag{69}$$

$$\int_{r_n}^{r_{n+1}} U_{z,n}^{II} \overline{\Psi}_{U_{z,n},m} r dr = 0, \tag{70}$$

$$\int_{r_n}^{r_{n+1}} u_{z,n}^{II} \overline{\Psi}_{u_{z,n},m} r dr = 0, \tag{71}$$

$$\int_{r_n}^{r_{n+1}} u_{r,n}^{II} \overline{\Psi}_{u_{r,n},m} r dr = 0, \tag{72}$$

where $\Psi_{p,m}$, $\Psi_{w_z,m}$, $\Psi_{U_{z,n},m}$, $\Psi_{u_{z,n},m}$, and $\Psi_{u_{r,n},m}$ are the weighting functions, and m is the number of modes ($m = 1$ to K). An appropriate choice of this weighting function will improve performance, and usually, an eigenfunction is chosen for each physical quantity. The motivation behind this method is to maximize the component of interest by exploiting orthogonality when performing integral calculations. In this study, the following weighting functions were used at the inlet ($z = 0$):

$$\Psi_{p,m} = \Phi_{p,m}^{I,-}, \tag{73}$$

$$\Psi_{w_z,m} = \Phi_{w_z,m}^{II,-}, \tag{74}$$

$$\Psi_{U_z,m} = \Phi_{U_z,m}^{II,+}, \tag{75}$$

$$\Psi_{u_z,m} = \Phi_{u_z,m}^{II,+}, \tag{76}$$

$$\Psi_{u_r,m} = \Phi_{u_r,m}^{II,+}. \tag{77}$$

Similarly, the weighting functions used at the outlet ($z = L$) are

$$\Psi_{p,m} = \Phi_{p,m}^{III,+}, \tag{78}$$

$$\Psi_{w_z,m} = \Phi_{w_z,m}^{II,-}, \tag{79}$$

$$\Psi_{U_z,m} = \Phi^{II,-}_{U_z,m}, \tag{80}$$

$$\Psi_{u_z,m} = \Phi^{II,-}_{u_z,m}, \tag{81}$$

$$\Psi_{u_r,m} = \Phi^{II,-}_{u_r,m}. \tag{82}$$

For a more in-depth discussion of the choice of weighting functions, see references [22,37].

At the inlet ($z = 0$), the boundary condition (68)–(72) in integral form can be simply expressed as follows:

$$\mathbf{P}^{I,+}\mathbf{A}^{I,+} + \mathbf{P}^{I,-}\mathbf{A}^{I,-} = \mathbf{P}^{II,+}\mathbf{A}^{II,+} + \mathbf{P}^{II,-}\mathbf{A}^{II,-}, \tag{83}$$

$$\mathbf{W}^{I,+}\mathbf{A}^{I,+} + \mathbf{W}^{I,-}\mathbf{A}^{I,-} = \mathbf{W}^{II,+}\mathbf{A}^{II,+} + \mathbf{W}^{II,-}\mathbf{A}^{II,-}, \tag{84}$$

$$\hat{\mathbf{W}}^{II,+}_n\mathbf{A}^{II,+} + \hat{\mathbf{W}}^{II,-}_n\mathbf{A}^{II,-} = 0. \tag{85}$$

where $\mathbf{P}^{I,+}$, $\mathbf{W}^{I,+}$, and $\hat{\mathbf{W}}^{II,+}_n$ are defined as follows, and the superscript * indicates complex transpose:

$$\mathbf{P}^{i,\pm} = \int_0^{r_1} \left(\mathbf{\Psi}_p\right)^* \mathbf{\Phi}^{i,\pm}_p r dr, \tag{86}$$

$$\mathbf{W}^{i,\pm} = \int_0^{r_1} \left(\mathbf{\Psi}_{w_z}\right)^* \mathbf{\Phi}^{i,\pm}_{w_z} r dr, \tag{87}$$

$$\hat{\mathbf{W}}^{II,\pm}_n = \int_{r_n}^{r_{n+1}} \left[\left(\mathbf{\Psi}_{U_{z,n}}\right)^* \mathbf{\Phi}^{II,\pm}_{U_{z,n}} + \left(\mathbf{\Psi}_{u_{z,n}}\right)^* \mathbf{\Phi}^{II,\pm}_{u_{z,n}} + \left(\mathbf{\Psi}_{u_{r,n}}\right)^* \mathbf{\Phi}^{II,\pm}_{u_{r,n}}\right] r dr, \tag{88}$$

where $\mathbf{\Psi}_p$, $\mathbf{\Psi}_{w_z}$, $\mathbf{\Psi}_{U_{z,n}}$, $\mathbf{\Psi}_{u_{z,n}}$, and $\mathbf{\Psi}_{u_{r,n}}$ are vectors of length K with each mode as an element.

Calculating the boundary conditions (70) through (72) separately would result in rounding errors and poor performance. Therefore, as in reference [22], this study employs a relaxation of the aforementioned condition by aggregating the three equations.

Now define the following notation,

$$\mathbf{X}_1 = \begin{pmatrix} \mathbf{P}^{I,-} & -\mathbf{P}^{II,+} \\ \mathbf{W}^{I,-} & -\mathbf{W}^{II,+} \\ 0 & -\hat{\mathbf{W}}^{II,+}_1 \\ 0 & -\hat{\mathbf{W}}^{II,+}_2 \\ \vdots & \vdots \\ 0 & -\hat{\mathbf{W}}^{II,+}_N \end{pmatrix}, \tag{89}$$

$$\mathbf{Y}_1 = \begin{pmatrix} -\mathbf{P}^{I,+} & \mathbf{P}^{II,-} \\ -\mathbf{W}^{I,+} & \mathbf{W}^{II,-} \\ 0 & \hat{\mathbf{W}}^{II,-}_1 \\ 0 & \hat{\mathbf{W}}^{II,-}_2 \\ \vdots & \vdots \\ 0 & \hat{\mathbf{W}}^{II,-}_N \end{pmatrix}. \tag{90}$$

Then, at the inlet ($z = 0$), the boundary conditions (83)–(85) are expressed in a simple matrix form as follows:

$$\mathbf{X}_1 \begin{pmatrix} \mathbf{A}^{I,-} \\ \mathbf{A}^{II,+} \end{pmatrix} = \mathbf{Y}_1 \begin{pmatrix} \mathbf{A}^{I,+} \\ \mathbf{A}^{II,-} \end{pmatrix}. \tag{91}$$

As previously stated, at the outlet ($z = L$), it is sufficient to multiply by the phase difference, like at the inlet, and is represented by

$$\mathbf{X}_2\mathbf{E}_X\begin{pmatrix}\mathbf{A}^{III,+}\\ \mathbf{A}^{II,-}\end{pmatrix} = \mathbf{Y}_2\mathbf{E}_Y\begin{pmatrix}\mathbf{A}^{III,-}\\ \mathbf{A}^{II,+}\end{pmatrix}, \tag{92}$$

where $\mathbf{X}_2$, $\mathbf{Y}_2$, $\mathbf{E}_X$, and $\mathbf{E}_Y$ are as follows:

$$\mathbf{X}_2 = \begin{pmatrix}\mathbf{P}^{III,+} & -\mathbf{P}^{II,-}\\ \mathbf{W}^{III,+} & -\mathbf{W}^{II,-}\\ 0 & -\hat{\mathbf{W}}_1^{II,-}\\ 0 & -\hat{\mathbf{W}}_2^{II,-}\\ \vdots & \vdots\\ 0 & -\hat{\mathbf{W}}_N^{II,-}\end{pmatrix}, \tag{93}$$

$$\mathbf{Y}_2 = \begin{pmatrix}-\mathbf{P}^{III,-} & \mathbf{P}^{II,+}\\ -\mathbf{W}^{III,-} & \mathbf{W}^{II,+}\\ 0 & \hat{\mathbf{W}}_1^{II,+}\\ 0 & \hat{\mathbf{W}}_2^{II,+}\\ \vdots & \vdots\\ 0 & \hat{\mathbf{W}}_N^{II,+}\end{pmatrix}. \tag{94}$$

$$\mathbf{E}_X = diag\left(e^{jk_{z,1}^{III,+}L},\ldots,e^{jk_{z,K}^{III,+}L},e^{jk_{z,1}^{II,-}L},\ldots,e^{jk_{z,K}^{II,-}L}\right), \tag{95}$$

$$\mathbf{E}_Y = diag\left(e^{jk_{z,1}^{III,-}L},\ldots,e^{jk_{z,K}^{III,-}L},e^{jk_{z,1}^{II,+}L},\ldots,e^{jk_{z,K}^{II,+}L}\right). \tag{96}$$

The purpose of this study is to solve (91) and (92). The method for solving the system of (91) and (92) is to start with the plane wave assumption $\mathbf{A}^{I,+} = [1,0,\ldots,0]^T$ and the assumption $\mathbf{A}^{III,-} = 0$ that there are no incoming waves at the outlet. Then, setting $\mathbf{A}^{II,-} = 0$ as (91) to obtain $\mathbf{A}^{II,+}$; then, substitute it into (92) to find $\mathbf{A}^{II,-}$, and then use it to solve (91) and repeat the process until convergence [22,38]. Equations (91) and (92) can be solved iteratively until convergence, and the solution is finally obtained. The reason for iteratively finding the solution is that the rounding error that occurs when solving the system by inversing the matrix is reduced repeatedly. It should be noted that the matrices $\mathbf{X}_1$ and $\mathbf{X}_2$ are not square, and, thus, the inverse operation cannot be performed directly. Instead, a pseudo-inverse matrix must be multiplied to obtain the desired result. Furthermore, it is necessary to multiply all the displacements by $(\rho_0 c_0 w)^2$ to make the displacements and pressures similar in magnitude [22]. Finally, the TL can be obtained from $\mathrm{TL} = -20\log_{10}\left|A_1^{III,+}\right|$ by setting $\left|A_1^{I,+}\right| = 1$.

4. Results and Discussions

To validate the proposed mode-matching method in this study, numerical tests were performed on silencers with single, double, and triple layers of poroelastic materials. The density and sound speed of air are 1.212 kg/m^3 and 342.208 m/s, respectively. The silencer used in the numerical test is 0.315 m long with r_1, r_2, and r_3 set to 0.037 m, 0.0566 m, and 0.0762 m, respectively [39]. The properties of the poroelastic materials are shown in Table 1. The names and properties of the poroelastic materials are taken from reference [40]. The poroelastic materials shown in Table 1 were chosen for two main reasons. First, we look at how the acoustic performance of the silencer varies with the placement of materials with different physical properties (e.g., strong rigidity or soft property). The second reason is to utilize results from the published literature to validate our proposed model [22,39,40]. There are no published results on the placement of poroelastic material in multiple layers,

and since the results of multiple layers composed of the same material should be the same as the results of a single layer, the dimensions and properties presented in the literature were utilized to validate the proposed model [22,39,40].

Table 1. Material properties [40].

Material	ϕ	σ (kNs/m^4)	α_∞	Λ (μm)	Λ' (μm)	ρ_1 (kg/m^3)	S (kPa)	ν
FM3	0.97	87	2.52	37	119	31	55	0.3
XFM	0.98	13.5	1.7	80	160	30	200	0.35
RGW2	0.99	9	1	192	384	16.3	220	0

The finite element analysis tool, COMSOL Multiphysics, was used to perform validation of TL model for a silencer with a single layer of poroelastic material. Based on a two-dimensional axisymmetric model, the Acoustic–Solid–Poroelastic Waves Interaction Interface in the Acoustics module was used for the computational analysis. The geometry was set as shown in Figure 1, and the Frequency Domain analysis of Pressure Acoustics was applied to the piping fluid, and the poroelastic material was subjected to the Poroelastic Waves analysis. The material properties listed in Table 1 were followed; boundary conditions were applied as mentioned in the previous sections, and fixed constraints were applied outside the pipe and silencer. The mesh was set separately for the poroelastic material and the piping fluid, with $\lambda/30$ for the poroelastic material and the poroelastic material-piping fluid interface, where fluid–structure interaction plays an important role, and $\lambda/6$ for the rest of the piping fluid, where λ is the wavelength.

4.1. Single Layer

First, the TL of a silencer composed of a single layer of porous material was calculated by the method proposed in this study. Referring to Table 1, the calculations (solid lines) were performed for three different porous materials with different material properties and directly compared with the results (markers) obtained by using the finite element numerical analysis tool, COMSOL Multiphysics, as shown in Figure 2.

Of the three materials, FM3 shows the behavior of a rigid foam-like material and effects due to the skeleton elasticity, as evidenced by several resonance peaks at 600–750 Hz. RGW2, on the other hand, depicts the behavior of wool, a common material for dissipation silencers for HVAC applications. XFM has properties between these two materials, showing the coupling effect between the fluid and solid phases of the poroelastic material, with a strong influence of the solid phase, especially in the resonance peak around 1500 Hz. Moreover, as illustrated in Figure 2, the outcomes are in substantial concordance with the FEM, thereby substantiating the analytic mode-matching method proposed in this study.

In general, foams such as XFM or FM3 can be viewed as porous materials with rigid skeletal frames, which have relatively high resonant frequencies and are known for their effectiveness in acoustic attenuation in the mid-to-high-frequency band. This rigid structure means that there is less torsion or deformation within the material when resonance occurs, so the energy is absorbed by the resonance and then quickly attenuated. As a result, the TL is high only at the resonance frequency, and the TL is stable at other frequencies. On the other hand, the resonance frequency of the TL of the silencer with XFM and FM3 is found in different frequency bands, and the TL of the silencer with XFM is higher than that of the silencer with FM3, showing a resonance characteristic around 1500 Hz. As shown in Table 1, this is due to the relatively higher viscous and thermal characteristic lengths and shear modulus of XFM compared to FM3.

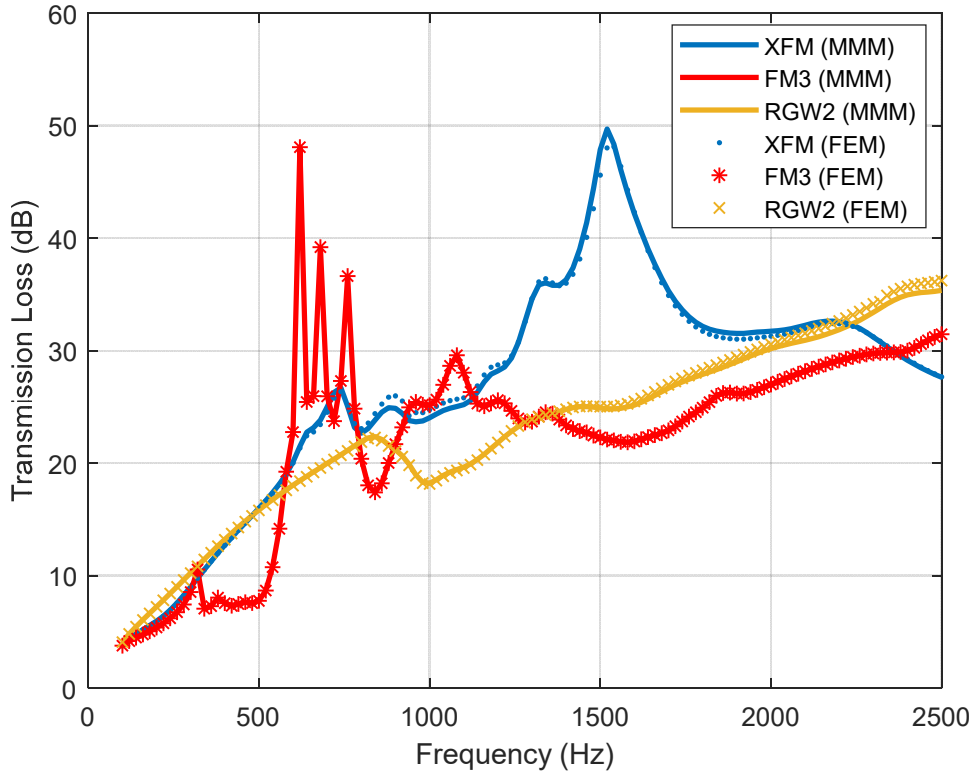

Figure 2. Comparison of mode-matching method (MMM) calculations (solid lines) and finite element method (FEM) results (markers) for the transmission loss (TL) of a silencer composed of a single-layer poroelastic material.

On the other hand, RGW2, which can be considered a soft material, has low stiffness due to its soft and flexible material characteristics, which is prone to resonance at low frequencies. In addition, the flexible structure of these materials makes it easy to deform the structure when resonance occurs, and the energy decays slowly as the deformation continues. This results in increased acoustic transmission losses in the resonant frequency band, but the slow decay allows for effects over a relatively wide frequency range. Based on the characteristics of these materials, the TL of the silencer with RGW2 shows no obvious resonance characteristics at low frequencies, but it has a relatively high TL in the frequency band below 500 Hz compared to the TL of the silencer with FM3, which has a higher stiffness. Moreover, an even transmission loss frequency characteristic is observed in the frequency band above 1500 Hz.

The multiple resonance peaks seen in the FM3 result indicate contributions from different modes and suggest that there may be several different mechanisms of acoustic energy dissipation, such as absorption or reflection. According to reference [41], fluid-borne modes contribute across the frequency band to the absorption mechanism of the silencer, while the absorption contribution of structure-borne modes is negligible at low frequencies, but the resonance peaks can occur where the contribution increases. As such, the resonance peak seen in Figure 2 can be interpreted as an increase in the influence of structure-borne modes under the overall contribution of fluid-borne modes. It can also be seen that for FM3, which has the smallest Young's modulus, the peak frequencies are reduced in the TL curves because the small Young's modulus causes a low resonance frequency of the skeleton vibration.

4.2. Double Layer

This section covers the case of double layers of poroelastic materials inside the silencer. The silencer specifications are the same as for the single-layer case, and the thickness of the poroelastic layers is set to be uniform. There is a total of nine ways to configure the

material in the double layers, allowing for overlap. Here, they are classified according to the type of poroelastic material located in the inner layer close to the center of the pipe and compared in Figure 3.

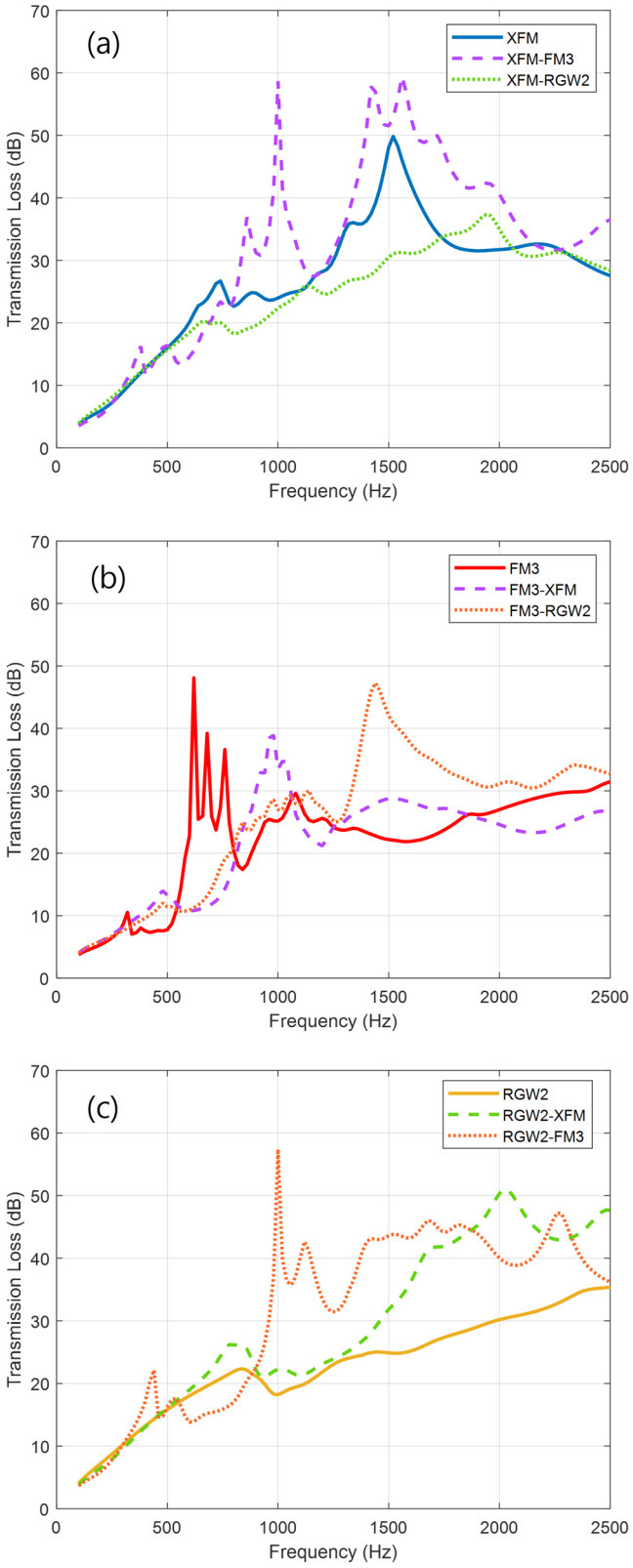

Figure 3. TL of a silencer composed of double-layer poroelastic materials. Configuration of (**a**) XFM, (**b**) FM3, and (**c**) RGW2 on the inner layer, respectively.

First, it should be noted that filling double layers inside the silencer with the same poroelastic material is effectively equivalent to filling one layer with a single poroelastic material, so comparing the solid lines in Figures 2 and 3 shows a perfect match. Next, the TLs of the silencer when the double layer is composed of different materials are shown in Figure 3a–c, respectively. For the purpose of convenience, the arrangement will be designated by the order of the material in the layers closer and farther from the center of the pipe. For example, XFM-FM3 considers a situation where XFM is filled in the layer closer to the center of the pipe, and FM3 is filled in the layer farther from the center of the pipe.

First, adding a stiffer material on the outside of the underlying poroelastic material (XFM-FM3) results in a stronger resonance characteristic due to the stiffness and seems to have the effect of shifting the resonance frequency to a lower frequency. On the contrary, adding a material with little stiffness (XFM-RGW2) weakens the resonance characteristics, lowering the peak values and shifting the resonance frequency to a high frequency. This is even more evident in Figure 3b, where the TL curve of the arrangement with the stiffest material, FM3, as the base material and the relatively weaker materials, XFM and RGW2, on the outside, shows that the resonant frequency characteristics are shifted to 1000 Hz and 1500 Hz, respectively. Figure 3c shows the result of placing XFM and FM3 in the outer layer with RGW2, a soft material, as the base, and the TL peak value with strong resonance characteristics can be seen accordingly.

4.3. Triple Layer

This section covers the case where a triple layer of poroelastic materials is used inside the silencer. The silencer specifications are the same as before, and the thickness of the pororoelastic layer is also set to be uniform. There is a total of 27 ways to configure the material for the triple layer, allowing for overlap. In the upper panels in Figure 4, the case of completely disparate material arrangements is presented first, which are incapable of overlapping with one another. As previously discussed, the materials have been classified according to their type and location in the inner layer, with nomenclature maintained consistently.

For Figure 4a,b, there is no noticeable difference compared to the double layer. However, a strong resonance around 1800 Hz is found in the XFM-RGW2-FM3 arrangement, and strong peaks around 1500 Hz and 2050 Hz are found in the FM3-XFM-RGW2 arrangement. Noteworthy is the characterization of the RGW2-XFM-FM3 arrangement shown in Figure 4c. A strong resonance characteristic appears around 1230 Hz and 1800 Hz, especially around 1800 Hz, where a very large TL of more than 70 dB is predicted to be obtained.

Similar characteristics are seen for this combination, allowing for the overlap shown in Figure 4d,e. Of interest here are the TL characteristics of the RGW2-RGW2-FM3 arrangement and the RGW2-FM3-RGW2 arrangement in Figure 4e. Both arrangements exhibit a very strong resonance peak near 2200 Hz with a large TL close to 80 dB. This is the strongest TL value among all possible combinations of single, double, and triple layers covered in this paper. The RGW2-RGW2-FM3 arrangement is a double layer with a larger inner layer thickness. Compared to the results of the similar arrangement RGW2-RGW2-XFM in Figure 4f, it can be expected that the TL at high frequencies will show a stronger resonance characteristic due to the larger impedance difference between the materials located in the inner and outer layers. In other words, it is expected that placing a soft material with a relatively small impedance difference from the material inside the pipe in the inner layer of the silencer and a material with a large impedance difference in the outer layer of the silencer can achieve a very large noise reduction effect at high frequencies.

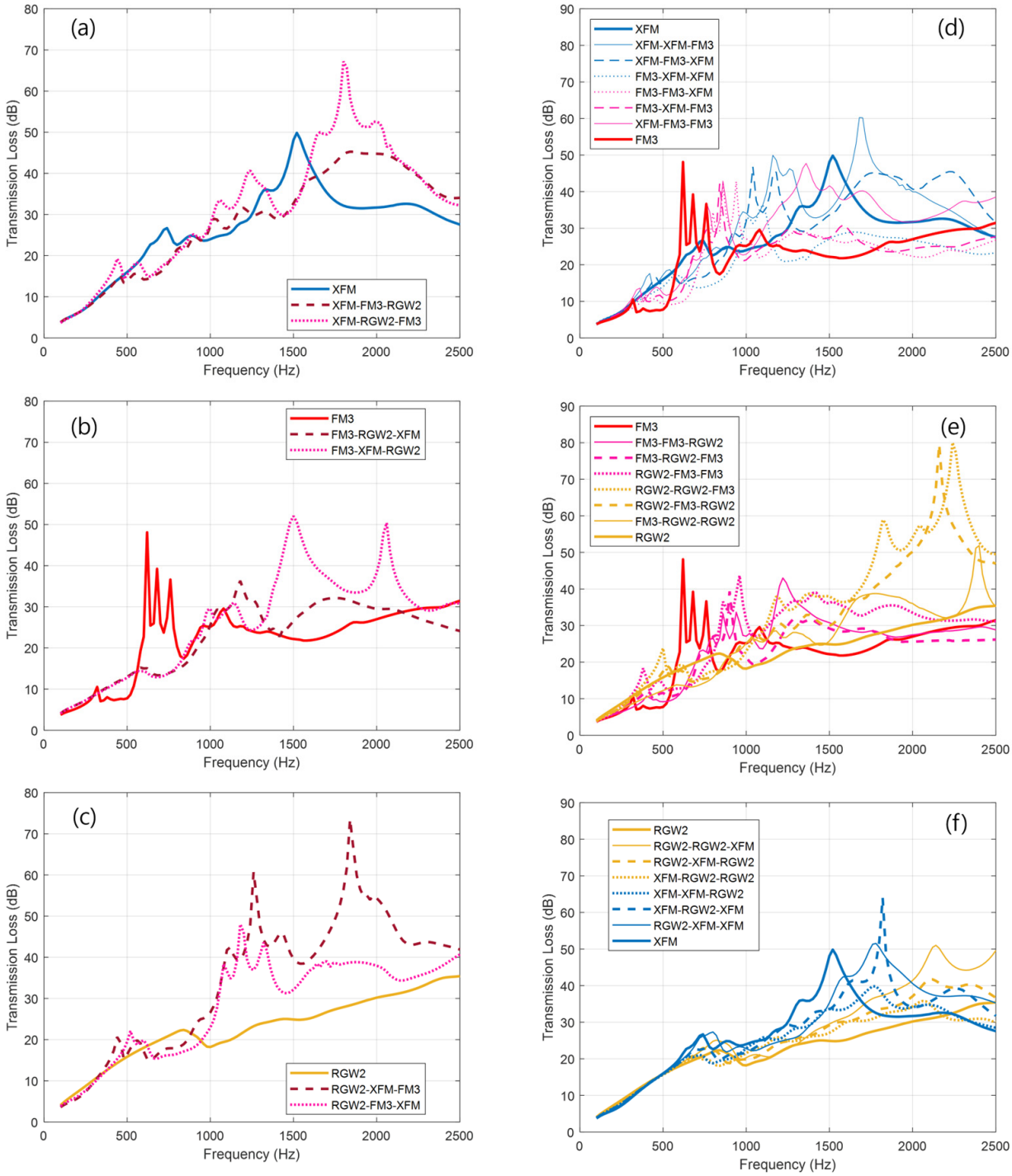

Figure 4. TL of a silencer composed of triple-layer poroelastic materials. Triple-layered with completely different materials: (**a**) XFM; (**b**) FM3; and (**c**) RGW2 on the inner layer, respectively. A combination of (**d**) XFM-FM3, (**e**) FM3-RGW2, and (**f**) RGW2-XFM, respectively.

5. Conclusions

This paper presents a methodology for modeling the acoustic performance of a silencer comprising multiple layers of poroelastic materials attached to the interior of the silencer. This methodology is founded upon the principles of a dissipative silencer, which is employed to mitigate the propagation of mid-to-high frequency piping noise in marine and offshore structural systems. It is anticipated that this approach will prove beneficial in scenarios where the dimensions of the silencer are enlarged or when it is deployed in specific

environments. In such instances, the poroelastic material may require the incorporation of multiple layers due to inherent manufacturing constraints.

First, this paper presents a mode-matching method for a silencer containing a multilayer poroelastic material, which is based on the mode-matching method for a silencer with a single layer of poroelastic material. This method introduces boundary conditions between poroelastic materials. The numerical experimental results were utilized to calculate the TL of double-layered and triple-layered poroelastic silencers. It was found that the results were consistent with those of the single-layer configuration when all layers were composed of the same material. The results obtained for the single layer were validated by comparison with the results obtained using the FEM, whose comparison was based on the published literature.

Furthermore, it was determined that the TL characteristics of the silencer are subject to alteration with changes in frequency, contingent upon the intrinsic properties of the poroelastic material. In particular, the TL characteristics of the silencer consisting of double and triple layers were summarized through numerical experiments. It was found that the TL characteristics of the silencer vary depending on the characteristics of each material when different materials are arranged. Materials with strong rigidity exhibit strong resonance characteristics; however, these characteristics can be mitigated by arranging them with soft materials.

The methodology presented in this paper allows for the economic analysis of acoustic characteristics in situations where multiple layers of poroelastic materials are constructed. This is due to the fact that it is more time-efficient than the FEM. Accordingly, it is anticipated that the design of silencers using poroelastic materials can be tailored to suit the specific requirements of the user or designer by taking into account the number of layers, thickness, and material configuration.

Author Contributions: Conceptualization, H.Y. and W.S.; methodology, H.Y. and W.S.; software, H.Y.; validation, H.Y. and W.S.; formal analysis, H.Y. and W.S.; writing—original draft preparation, H.Y.; writing—review and editing, H.Y. and W.S.; supervision, W.S.; funding acquisition, H.Y. All authors have read and agreed to the published version of the manuscript.

Funding: This work was supported by the National Research Foundation of Korea (NRF) grant funded by the Korea government (MSIT) (No. 2022R1A2C1092717).

Institutional Review Board Statement: Not applicable.

Informed Consent Statement: Not applicable.

Data Availability Statement: The original contributions presented in this study are included in this article; further inquiries can be directed to the corresponding author.

Conflicts of Interest: The authors declare no conflicts of interest.

Nomenclature

N	Number of layers of poroelastic material
L	Length of silencer
r_N	Distance to N-th poroelastic material from the center of pipe
t	Time
c_0	Speed of sound in the air
k_0	Wavenumber in the air
ω	Angular frequency
λ	Wavelength
k_z	Wavenumber in the z-direction
p	Acoustic pressure in the air
ρ_0	Density of the air
ϕ_0	Displacement potential of the compressional wave in the air
ϕ_1	Displacement potential of the first compressional wave in the poroelastic material

ϕ_2	Displacement potential of the second compressional wave in the poroelastic material
ψ	Displacement potential of the shear wave in the poroelastic material
$\mathbf{w}$	Particle perturbation displacement within the fluid
$\mathbf{u}$	Displacement of the solid in the poroelastic material
$\mathbf{U}$	Average displacement of the fluid in the poroelastic material
μ_1	Ratio of amplitudes between the compressional waves in the fluid
μ_2	Ratio of amplitudes between the compressional waves in the solid
μ_3	Ratio of amplitudes between the shear waves
m	Mode number
n	Index of poroelastic material layer
σ_{ij}^s	Stress in solid phase for the poroelastic material
σ_{ij}^f	Stress in fluid phase for the poroelastic material
σ_{ij}^t	Total stress
p_p	Pore pressure
ϕ	Porosity
S	Complex shear modulus of the skeleton of the poroelastic material
K_b	Bulk modulus of the frame
ν	Poisson's ratio
K_f	Bulk modulus of the fluid
ρ_f	Density of the fluid
α_∞	Tortuosity
σ	Flow resistivity
η	Viscosity of the air
κ	Thermal conductivity of the air
C_p	Static pressure specific heat
Λ	Viscous characteristic length
Λ'	Thermal characteristic length
γ	Specific heat ratio
P_0	Atmospheric pressure
k_0'	Static thermal conductivity
ρ_s	Density of the frame
ρ_1	Apparent density of the frame considering the porosity
$\mathbf{n}$	Normal vector
J_m	m-th order Bessel function of the first kind
Y_m	m-th order Bessel function of the second kind
$\Phi_{p,m}^{i,\pm}$	m-th eigenfunction of pressure
$A_m^{i,\pm}$	Coefficient preceding the m-th eigenfunction
$\Phi_{w_z}^{i,\pm}$	Eigenfunction of displacement of the air
$\Phi_{U_{z,n}}^{i,\pm}$	Eigenfunction of the fluid displacement in the poroelatic material
$\Phi_{u_{z,n}}^{i,\pm}$, $\Phi_{u_{r,n}}^{i,\pm}$	Eigenfunction of the solid displacement in the poroelatic material
Ψ	Weighting function
diag	Diagonal matrix
tr	Trace matrix
FEM	Finite element method
HVAC	Heating, ventilation, and air conditioning
JCAL model	Johnson-Champous-Allard-Lafarge model
TL	Transmission loss

Appendix A

For the boundary condition (39) for a silencer with N layers of poroelastic material, the components of the matrix $\mathbf{C}$ are given below. The subscript n indicates the order of the layers close to the pipe ($n = 1,\ 2,\ 3, \ldots,\ N-1$).

$$C_{1,1} = -H_{1,1} J_0(k_{1r,1} r_1) + \frac{2S_{,1} k_{1r,1}}{r_1} J_1(k_{1r,1} r_1), \tag{A1}$$

$$C_{1,2} = -H_{1,1}Y_0(k_{1r,1}r_1) + \frac{2S_{,1}k_{1r,1}}{r_1}Y_1(k_{1r,1}r_1), \tag{A2}$$

$$C_{1,3} = -H_{2,1}J_0(k_{2r,1}r_1) + \frac{2S_{,1}k_{2r,1}}{r_1}J_1(k_{2r,1}r_1), \tag{A3}$$

$$C_{1,4} = -H_{2,1}Y_0(k_{2r,1}r_1) + \frac{2S_{,1}k_{2r,1}}{r_1}Y_1(k_{2r,1}r_1), \tag{A4}$$

$$C_{1,5} = 2S_{,1}jk_z\left[-\frac{1}{r_1}J_1(k_{3r,1}r_1) + k_{3r,1}J_0(k_{3r,1}r_1)\right], \tag{A5}$$

$$C_{1,5} = 2S_{,1}jk_z\left[-\frac{1}{r_1}J_1(k_{3r,1}r_1) + k_{3r,1}J_0(k_{3r,1}r_1)\right], \tag{A6}$$

$$C_{1,6N+1} = \rho_0 c_0^2 k_0^2 J_0(k_{0r}r_1), \tag{A7}$$

$$C_{2,1} = -2jS_{,1}k_z J_1(k_{1r,1}r_1)k_{1r,1}, \tag{A8}$$

$$C_{2,2} = -2jS_{,1}k_z Y_1(k_{1r,1}r_1)k_{1r,1}, \tag{A9}$$

$$C_{2,3} = -2jS_{,1}k_z J_1(k_{2r,1}r_1)k_{2r,1}, \tag{A10}$$

$$C_{2,4} = -2jS_{,1}k_z Y_1(k_{2r,1}r_1)k_{2r,1}, \tag{A11}$$

$$C_{2,5} = S_{,1}J_1(k_{3r,1}r_1)\left(-k_z^2 + k_{3r,1}^2\right), \tag{A12}$$

$$C_{2,6} = S_{,1}Y_1(k_{3r,1}r_1)\left(-k_z^2 + k_{3r,1}^2\right), \tag{A13}$$

$$C_{3,1} = \frac{k_{1,1}^2}{\phi_{,1}}(Q_{,1} + R_{,1}\mu_{1,1})J_0(k_{1r,1}r_1), \tag{A14}$$

$$C_{3,2} = \frac{k_{1,1}^2}{\phi_{,1}}(Q_{,1} + R_{,1}\mu_{1,1})Y_0(k_{1r,1}r_1), \tag{A15}$$

$$C_{3,3} = \frac{k_{2,1}^2}{\phi_{,1}}(Q_{,1} + R_{,1}\mu_{2,1})J_0(k_{2r,1}r_1), \tag{A16}$$

$$C_{3,4} = \frac{k_{2,1}^2}{\phi_{,1}}(Q_{,1} + R_{,1}\mu_{2,1})Y_0(k_{2r,1}r_1), \tag{A17}$$

$$C_{3,6N+1} = -\rho_0 c_0^2 k_0^2 J_0(k_{0r}r_1), \tag{A18}$$

$$C_{4,1} = -k_{1r,1}(\phi_{,1}\mu_{1,1} - \phi_{,1} + 1)J_1(k_{1r,1}r_1), \tag{A19}$$

$$C_{4,2} = -k_{1r,1}(\phi_{,1}\mu_{1,1} - \phi_{,1} + 1)Y_1(k_{1r,1}r_1), \tag{A20}$$

$$C_{4,3} = -k_{2r,1}(\phi_{,1}\mu_{2,1} - \phi_{,1} + 1)J_1(k_{2r,1}r_1), \tag{A21}$$

$$C_{4,4} = -k_{2r,1}(\phi_{,1}\mu_{2,1} - \phi_{,1} + 1)Y_1(k_{2r,1}r_1), \tag{A22}$$

$$C_{4,5} = jk_z(\phi_{,1}\mu_{3,1} - \phi_{,1} + 1)J_1(k_{3r,1}r_1), \tag{A23}$$

$$C_{4,6} = jk_z(\phi_{,1}\mu_{3,1} - \phi_{,1} + 1)Y_1(k_{3r,1}r_1), \tag{A24}$$

$$C_{4,6N+1} = k_{0r} J_1(k_{0r} r_1), \tag{A25}$$

$$C_{5,6N-5} = -k_{1r,N} J_1(k_{1r,N} r_{N+1}), \tag{A26}$$

$$C_{5,6N-4} = -k_{1r,N} Y_1(k_{1r,N} r_{N+1}), \tag{A27}$$

$$C_{5,6N-3} = -k_{2r,N} J_1(k_{2r,N} r_{N+1}), \tag{A28}$$

$$C_{5,6N-2} = -k_{2r,N} Y_1(k_{2r,N} r_{N+1}), \tag{A29}$$

$$C_{5,6N-1} = jk_z J_1(k_{3r,N} r_{N+1}), \tag{A30}$$

$$C_{5,6N} = jk_z Y_1(k_{3r,N} r_{N+1}), \tag{A31}$$

$$C_{6,6N-5} = jk_z J_0(k_{1r,N} r_{N+1}), \tag{A32}$$

$$C_{6,6N-4} = jk_z Y_0(k_{1r,N} r_{N+1}), \tag{A33}$$

$$C_{6,6N-3} = jk_z J_0(k_{2r,N} r_{N+1}), \tag{A34}$$

$$C_{6,6N-2} = jk_z Y_0(k_{2r,N} r_{N+1}), \tag{A35}$$

$$C_{6,6N-1} = -k_{3r,N} J_0(k_{3r,N} r_{N+1}), \tag{A36}$$

$$C_{6,6N} = -k_{3r,N} Y_0(k_{3r,N} r_{N+1}), \tag{A37}$$

$$C_{7,6N-5} = -k_{1r,N} \mu_{1,N} J_1(k_{1r,N} r_{N+1}), \tag{A38}$$

$$C_{7,6N-4} = -k_{1r,N} \mu_{1,N} Y_1(k_{1r,N} r_{N+1}), \tag{A39}$$

$$C_{7,6N-3} = -k_{2r,N} \mu_{2,N} J_1(k_{2r,N} r_{N+1}), \tag{A40}$$

$$C_{7,6N-2} = -k_{2r,N} \mu_{2,N} Y_1(k_{2r,N} r_{N+1}), \tag{A41}$$

$$C_{7,6N-1} = Jk_z \mu_{3,N} J_1(k_{3r,N} r_{N+1}), \tag{A42}$$

$$C_{7,6N} = Jk_z \mu_{3,N} Y_1(k_{3r,N} r_{N+1}), \tag{A43}$$

$$C_{6n+2,6n-5} = -H_{1,n} J_0(k_{1r,n} r_{n+1}) + \frac{2S_{,n} k_{1r,n}}{r_{n+1}} J_1(k_{1r,n} r_{n+1}), \tag{A44}$$

$$C_{6n+2,6n-4} = -H_{1,n} Y_0(k_{1r,n} r_{n+1}) + \frac{2S_{,n} k_{1r,n}}{r_{n+1}} Y_1(k_{1r,n} r_{n+1}), \tag{A45}$$

$$C_{6n+2,6n-3} = -H_{2,n} J_0(k_{2r,n} r_{n+1}) + \frac{2S_{,n} k_{2r,n}}{r_{n+1}} J_1(k_{2r,n} r_{n+1}), \tag{A46}$$

$$C_{6n+2,6n-2} = -H_{2,n} Y_0(k_{2r,n} r_{n+1}) + \frac{2S_{,n} k_{2r,n}}{r_{n+1}} Y_1(k_{2r,n} r_{n+1}), \tag{A47}$$

$$C_{6n+2,6n-1} = 2S_{,n} jk_z \left[-\frac{J_1(k_{3r,n} r_{n+1})}{r_{n+1}} + k_{3r,n} J_0(k_{3r,n} r_{n+1}) \right], \tag{A48}$$

$$C_{6n+2,6n} = 2S_{,n} jk_z \left[-\frac{Y_1(k_{3r,n} r_{n+1})}{r_{n+1}} + k_{3r,n} Y_0(k_{3r,n} r_{n+1}) \right], \tag{A49}$$

$$C_{6n+2,6n+1} = H_{1,n+1}J_0(k_{1r,n+1}r_{n+1}) - \frac{2S_{,n+1}k_{1r,n+1}}{r_{n+1}}J_1(k_{1r,n+1}r_{n+1}), \tag{A50}$$

$$C_{6n+2,6n+2} = H_{1,n+1}Y_0(k_{1r,n+1}r_{n+1}) - \frac{2S_{,n+1}k_{1r,n+1}}{r_{n+1}}Y_1(k_{1r,n+1}r_{n+1}), \tag{A51}$$

$$C_{6n+2,6n+3} = H_{2,n+1}J_0(k_{2r,n+1}r_{n+1}) - \frac{2S_{,n+1}k_{2r,n+1}}{r_{n+1}}J_1(k_{2r,n+1}r_{n+1}), \tag{A52}$$

$$C_{6n+2,6n+4} = H_{2,n+1}Y_0(k_{2r,n+1}r_{n+1}) - \frac{2S_{,n+1}k_{2r,n+1}}{r_{n+1}}Y_1(k_{2r,n+1}r_{n+1}), \tag{A53}$$

$$C_{6n+2,6n+5} = 2S_{,n+1}jk_z\left[\frac{J_1(k_{3r,n+1}r_{n+1})}{r_{n+1}} - k_{3r,n+1}J_0(k_{3r,n+1}r_{n+1})\right], \tag{A54}$$

$$C_{6n+2,6n+6} = 2S_{,n+1}jk_z\left[\frac{Y_1(k_{3r,n+1}r_{n+1})}{r_{n+1}} - k_{3r,n+1}Y_0(k_{3r,n+1}r_{n+1})\right], \tag{A55}$$

$$C_{6n+3,6n-5} = -2jS_{,n}k_zJ_1(k_{1r,n}r_{n+1})k_{1r,n}, \tag{A56}$$

$$C_{6n+3,6n-4} = -2jS_{,n}k_zY(k_{1r,n}r_{n+1})k_{1r,n}, \tag{A57}$$

$$C_{6n+3,6n-3} = -2jS_{,n}k_zJ_1(k_{2r,n}r_{n+1})k_{2r,n}, \tag{A58}$$

$$C_{6n+3,6n-2} = -2jS_{,n}k_zY_1(k_{2r,n}r_{n+1})k_{2r,n}, \tag{A59}$$

$$C_{6n+3,6n-1} = S_{,n}J_1(k_{3r,n}r_{n+1})\left(-k_z^2 + k_{3r,n}^2\right), \tag{A60}$$

$$C_{6n+3,6n} = S_{,n}Y_1(k_{3r,n}r_{n+1})\left(-k_z^2 + k_{3r,n}^2\right), \tag{A61}$$

$$C_{6n+3,6n+1} = 2jS_{,n+1}k_zJ_1(k_{1r,n+1}r_{n+1})k_{1r,n+1}, \tag{A62}$$

$$C_{6n+3,6n+2} = 2jS_{,n+1}k_zY_1(k_{1r,n+1}r_{n+1})k_{1r,n+1}, \tag{A63}$$

$$C_{6n+3,6n+3} = 2jS_{,n+1}k_zJ_1(k_{2r,n+1}r_{n+1})k_{2r,n+1}, \tag{A64}$$

$$C_{6n+3,6n+4} = 2jS_{,n+1}k_zY_1(k_{2r,n+1}r_{n+1})k_{2r,n+1}, \tag{A65}$$

$$C_{6n+3,6n+5} = S_{,n+1}J_1(k_{3r,n+1}r_{n+1})\left(k_z^2 - k_{3r,n+1}^2\right), \tag{A66}$$

$$C_{6n+3,6n+6} = S_{,n+1}Y_1(k_{3r,n+1}r_{n+1})\left(k_z^2 - k_{3r,n+1}^2\right), \tag{A67}$$

$$C_{6n+4,6n-5} = -k_{1r,n}J_1(k_{1r,n}r_{n+1}), \tag{A68}$$

$$C_{6n+4,6n-4} = -k_{1r,n}Y_1(k_{1r,n}r_{n+1}), \tag{A69}$$

$$C_{6n+4,6n-3} = -k_{2r,n}J_1(k_{2r,n}r_{n+1}), \tag{A70}$$

$$C_{6n+4,6n-2} = -k_{2r,n}Y_1(k_{2r,n}r_{n+1}), \tag{A71}$$

$$C_{6n+4,6n-1} = jk_zJ_1(k_{3r,n}r_{n+1}), \tag{A72}$$

$$C_{6n+4,6n} = jk_zY_1(k_{3r,n}r_{n+1}), \tag{A73}$$

$$C_{6n+4,6n+1} = k_{1r,n+1}J_1(k_{1r,n+1}r_{n+1}), \tag{A74}$$

$$C_{6n+4,6n+2} = k_{1r,n+1} Y_1(k_{1r,n+1} r_{n+1}), \tag{A75}$$

$$C_{6n+4,6n+3} = k_{2r,n+1} J_1(k_{2r,n+1} r_{n+1}), \tag{A76}$$

$$C_{6n+4,6n+4} = k_{2r,n+1} Y_1(k_{2r,n+1} r_{n+1}), \tag{A77}$$

$$C_{6n+4,6n+5} = -jk_z J_1(k_{3r,n+1} r_{n+1}), \tag{A78}$$

$$C_{6n+4,6n+6} = -jk_z Y_1(k_{3r,n+1} r_{n+1}), \tag{A79}$$

$$C_{6n+5,6n-5} = jk_z J_0(k_{1r,n} r_{n+1}), \tag{A80}$$

$$C_{6n+5,6n-4} = jk_z Y_0(k_{1r,n} r_{n+1}), \tag{A81}$$

$$C_{6n+5,6n-3} = k_z J_0(k_{2r,n} r_{n+1}), \tag{A82}$$

$$C_{6n+5,6n-2} = jk_z Y_0(k_{2r,n} r_{n+1}), \tag{A83}$$

$$C_{6n+5,6n-1} = -k_{3r,n} J_0(k_{3r,n} r_{n+1}), \tag{A84}$$

$$C_{6n+5,6n} = -k_{3r,n} Y_0(k_{3r,n} r_{n+1}), \tag{A85}$$

$$C_{6n+5,6n+1} = -jk_z J_0(k_{1r,n+1} r_{n+1}), \tag{A86}$$

$$C_{6n+5,6n+2} = -jk_z Y_0(k_{1r,n+1} r_{n+1}), \tag{A87}$$

$$C_{6n+5,6n+3} = -jk_z J_0(k_{2r,n+1} r_{n+1}), \tag{A88}$$

$$C_{6n+5,6n+4} = -jk_z Y_0(k_{2r,n+1} r_{n+1}), \tag{A89}$$

$$C_{6n+5,6n+5} = k_{3r,n+1} J_0(k_{3r,n+1} r_{n+1}), \tag{A90}$$

$$C_{6n+5,6n+6} = k_{3r,n+1} Y_0(k_{3r,n+1} r_{n+1}), \tag{A91}$$

$$C_{6n+6,6n-5} = \frac{k_{1,n}^2}{\phi_{,n}} (Q_{,n} + R_{,n} \mu_{1,n}) J_0(k_{1r,n} r_{n+1}), \tag{A92}$$

$$C_{6n+6,6n-4} = \frac{k_{1,n}^2}{\phi_{,n}} (Q_{,n} + R_{,n} \mu_{1,n}) Y_0(k_{1r,n} r_{n+1}), \tag{A93}$$

$$C_{6n+6,6n-3} = \frac{k_{2,n}^2}{\phi_{,n}} (Q_{,n} + R_{,n} \mu_{2,n}) J_0(k_{2r,n} r_{n+1}), \tag{A94}$$

$$C_{6n+6,6n-2} = \frac{k_{2,n}^2}{\phi_{,n}} (Q_{,n} + R_{,n} \mu_{2,n}) Y_0(k_{2r,n} r_{n+1}), \tag{A95}$$

$$C_{6n+6,6n+1} = \frac{k_{1,n+1}^2}{\phi_{,n+1}} (Q_{,n+1} + R_{,n+1} \mu_{1,n+1}) J_0(k_{1r,n+1} r_{n+1}), \tag{A96}$$

$$C_{6n+6,6n+2} = \frac{k_{1,n+1}^2}{\phi_{,n+1}} (Q_{,n+1} + R_{,n+1} \mu_{1,n+1}) Y_0(k_{1r,n+1} r_{n+1}), \tag{A97}$$

$$C_{6n+6,6n+3} = \frac{k_{2,n+1}^2}{\phi_{,n+1}} (Q_{,n+1} + R_{,n+1} \mu_{2,n+1}) J_0(k_{2r,n+1} r_{n+1}), \tag{A98}$$

$$C_{6n+6,6n+4} = \frac{k_{2,n+1}^2}{\phi_{,n+1}}(Q_{,n+1} + R_{,n+1}\mu_{2,n+1})Y_0(k_{2r,n+1}r_{n+1}), \quad \text{(A99)}$$

$$C_{6n+7,6n-5} = -k_{1r,n}\phi_{,n}(\mu_{1,n} - 1)J_1(k_{1r,n}r_{n+1}), \quad \text{(A100)}$$

$$C_{6n+7,6n-4} = -k_{1r,n}\phi_{,n}(\mu_{1,n} - 1)Y_1(k_{1r,n}r_{n+1}), \quad \text{(A101)}$$

$$C_{6n+7,6n-3} = -k_{2r,n}\phi_{,n}(\mu_{2,n} - 1)J_1(k_{2r,n}r_{n+1}), \quad \text{(A102)}$$

$$C_{6n+7,6n-2} = -k_{2r,n}\phi_{,n}(\mu_{2,n} - 1)Y_1(k_{2r,n}r_{n+1}), \quad \text{(A103)}$$

$$C_{6n+7,6n-1} = jk_z\phi_{,n}(\mu_{3,n} - 1)J_1(k_{3r,n}r_{n+1}), \quad \text{(A104)}$$

$$C_{6n+7,6n} = jk_z\phi_{,n}(\mu_{3,n} - 1)Y_1(k_{3r,n}r_{n+1}), \quad \text{(A105)}$$

$$C_{6n+7,6n+1} = k_{1r,n+1}\phi_{,n+1}(\mu_{1,n+1} - 1)J_1(k_{1r,n+1}r_{n+1}), \quad \text{(A106)}$$

$$C_{6n+7,6n+2} = k_{1r,n+1}\phi_{,n+1}(\mu_{1,n+1} - 1)Y_1(k_{1r,n+1}r_{n+1}), \quad \text{(A107)}$$

$$C_{6n+7,6n+3} = k_{2r,n+1}\phi_{,n+1}(\mu_{2,n+1} - 1)J_1(k_{2r,n+1}r_{n+1}), \quad \text{(A108)}$$

$$C_{6n+7,6n+4} = k_{2r,n+1}\phi_{,n+1}(\mu_{2,n+1} - 1)Y_1(k_{2r,n+1}r_{n+1}), \quad \text{(A109)}$$

$$C_{6n+7,6n+5} = -jk_z\phi_{,n+1}(\mu_{3,n+1} - 1)J_1(k_{3r,n+1}r_{n+1}), \quad \text{(A110)}$$

$$C_{6n+7,6n+6} = -jk_z\phi_{,n+1}(\mu_{3,n+1} - 1)Y_1(k_{3r,n+1}r_{n+1}), \quad \text{(A111)}$$

$$H_{i,n} = ((R_{,n} + Q_{,n})\mu_{i,n} + Q_{,n} + A_{,n})k_{i,n}^2 + 2S_{,n}k_{ir,n}^2 \quad \text{(A112)}$$

References

1. Diviacco, P.; Nadali, A.; Iurcev, M.; Burca, M.; Carbajales, R.; Gangale, M.; Busato, A.; Brunetti, F.; Grio, L.; Viola, A.; et al. Underwater noise monitoring with real-time and low-cost systems, (The CORMA Experience). *J. Mar. Sci. Eng.* **2021**, *9*, 390. [CrossRef]
2. Parsons, M.J.; Erbe, C.; Meekan, M.G.; Parsons, S.K. A review and meta-analysis of underwater noise radiated by small (<25 m length) vessels. *J. Mar. Sci. Eng.* **2021**, *9*, 827. [CrossRef]
3. Li, Y.; Zhang, C.; Zhou, Y. A novel denoising method for ship-radiated noise. *J. Mar. Sci. Eng.* **2023**, *11*, 1730. [CrossRef]
4. Juretzek, C.; Schmidt, B.; Boethling, M. Turning scientific knowledge into regulation: Effective measures for noise mitigation of pile driving. *J. Mar. Sci. Eng.* **2021**, *9*, 819. [CrossRef]
5. Jesus, S.M.; Soares, C.; Romagosa, M.; Cascão, I.; Duarte, R.; Zabel, F.; Silva, M.A. A methodology for shipping noise field calibration and excess noise estimation: The Azores case study. *J. Mar. Sci. Eng.* **2022**, *10*, 1763. [CrossRef]
6. Munjal, M.L. *Acoustics of Ducts and Mufflers*, 2nd ed.; John Wiley & Sons: Bognor Regis, UK, 2014; pp. 233–265.
7. Xu, M.B.; Selamet, A.; Lee, I.-J.; Huff, N.T. Sound attenuation in dissipative expansion chambers. *J. Sound Vib.* **2004**, *272*, 1125–1133. [CrossRef]
8. Potente, D. General design principles for an automotive muffler. In Proceedings of the ACOUSTICS, Busselton, AUS, Australia, 9–11 November 2005.
9. Craggs, A. A finite element method for modelling dissipative mufflers with a locally reactive lining. *J. Sound Vib.* **1977**, *54*, 285–296. [CrossRef]
10. Peat, K.S. A transfer matrix for an absorption silencer element. *J. Sound Vib.* **1991**, *146*, 353–360. [CrossRef]
11. Hergli, K.; Mosbahi, H. Transmission loss prediction of dissipative silencers using the finite element method. In Proceedings of the 2024 International Conference on Control, Automation and Diagnosis (ICCAD), Paris, France, 15–17 May 2024.
12. Benchea, M.; Bujoreanu, C.; Ianus, G. Acoustic Performance of Some Lined Dissipative Silencers. In *Innovations in Mechanical Engineering*; Machado, J., Soares, F., Trojanowska, J., Ottaviano, E., Eds.; Springer International Publishing: Cham, Switzerland, 2022; pp. 302–311.
13. Jokandan, M.R.; Ahmadi, S. Study of acoustic and aerodynamic performance of reactive silencer with different configurations: Theoretical, modeling and experimental. *Heliyon* **2023**, *9*, e20058. [CrossRef]
14. Zhou, X.; Ji, Z. Sound attenuation analysis of water filled perforated pipe silencers using three-dimensional time-domain computational fluid dynamics approach. *Adv. Mech. Eng.* **2016**, *8*, 1687814016642955. [CrossRef]

15. Xuan, L.-K.; Liu, Y.; Gong, J.-F.; Ming, P.-J.; Ruan, Z.-Q. A time-domain finite volume method for the prediction of water muffler transmission loss considering elastic walls. *Adv. Mech. Eng.* **2017**, *9*, 1687814017690068. [CrossRef]
16. Liu, B.; Yang, L. Transmission of Low-Frequency Acoustic Waves in Seawater Piping Systems with Periodical and Adjustable Helmholtz Resonator. *J. Mar. Sci. Eng.* **2017**, *5*, 56. [CrossRef]
17. Delany, M.E.; Bazley, E.N. Acoustical properties of fibrous absorbent materials. *Appl. Acoust.* **1970**, *3*, 105–116. [CrossRef]
18. Selamet, A.; Xu, M.B.; Lee, I.-J.; Huff, N.T. Analytical approach for sound attenuation in perforated dissipative silencers with inlet/outlet extensions. *J. Acoust. Soc. Am.* **2005**, *117*, 2078–2089. [CrossRef] [PubMed]
19. Biot, M.A. Theory of propagation of elastic waves in a fluid-saturated porous solid. I. Low-frequency range. *J. Acoust. Soc. Am.* **1956**, *28*, 168–178. [CrossRef]
20. Biot, M.A. Theory of propagation of elastic waves in a fluid-saturated porous solid. II. Higher frequency range. *J. Acoust. Soc. Am.* **1956**, *28*, 179–191. [CrossRef]
21. Allard, J.; Atalla, N. *Propagation of Sound in Porous Media: Modeling Sound Absorbing Materials*, 2nd ed.; John Wiley & Sons: Bognor Regis, UK, 2009; pp. 73–110.
22. Nennig, B.; Perrey-Debain, E.; Ben Tahar, M. A mode matching method for modeling dissipative silencers lined with poroelastic materials and containing mean flow. *J. Acoust. Soc. Am.* **2010**, *128*, 3308–3320. [CrossRef]
23. Selamet, A.; Xu, M.B.; Lee, I.-J.; Huff, N.T. Dissipative expansion chambers with two concentric layers of fibrous material. *Int. J. Veh. Noise Vib.* **2005**, *1*, 341–357. [CrossRef]
24. Veerababy, D.; Venkatesham, B. Green's function approach for the transmission loss of concentrically multi-layered circular dissipative chamber. *J. Acoust. Soc. Am.* **2020**, *147*, 867–876. [CrossRef]
25. Gazis, D.C. Three-dimensional investigation of the propagation of waves in hollow circular cylinders. I. Analytical foundation. *J. Acoust. Soc. Am.* **1959**, *31*, 568–573. [CrossRef]
26. Debergue, P.; Panneton, R.; Atalla, N. Boundary conditions for the weak formulation of the mixed (u, p) poroelasticity problem. *J. Acoust. Soc. Am.* **1999**, *106*, 2383–2390. [CrossRef]
27. Bilawchuk, S.; Fyfe, K.R. Comparison and implementation of the various numerical methods used for calculating transmission loss in silencer systems. *Appl. Acoust.* **2003**, *64*, 903–916. [CrossRef]
28. Mehdizadeh, O.Z.; Paraschivoiu, M. A three-dimensional finite element approach for predicting the transmission loss in mufflers and silencers with no mean flow. *Appl. Acoust.* **2005**, *66*, 902–918. [CrossRef]
29. Ji, Z.L. Boundary element acoustic analysis of hybrid expansion chamber silencers with perforated facing. *Eng. Anal. Boundary Elem.* **2010**, *34*, 690–696. [CrossRef]
30. Kirby, R. Transmission loss predictions for dissipative silencers of arbitrary cross section in the presence of mean flow. *J. Acoust. Soc. Am.* **2003**, *114*, 200–209. [CrossRef]
31. Albelda, J.; Denia, F.D.; Torres, M.I.; Fuenmayor, F.J. A transversal substructuring mode matching method applied to the acoustic analysis of dissipative silencers. *J. Sound Vib.* **2007**, *303*, 614–631. [CrossRef]
32. Kirby, R. A comparison between analytic and numerical methods for modeling automotive dissipative silencers with mean flow. *J. Sound Vib.* **2009**, *325*, 565–582. [CrossRef]
33. Fang, Z.; Ji, Z.L. Acoustic attenuation analysis of expansion chambers with extended inlet/outlet. *Noise Control Eng. J.* **2013**, *61*, 240–249. [CrossRef]
34. Fang, Z.; Ji, Z.L. Numerical mode matching approach for acoustic attenuation predictions of double-chamber perforated tube dissipative silencers with mean flow. *J. Comput. Acoust.* **2014**, *22*, 678–702. [CrossRef]
35. Liu, G.R.; Gu, Y.T. *An Introduction to Meshfree Methods and Their Programming*; Springer: New York, NY, USA, 2005; pp. 37–53.
36. Fang, Z.; Liu, C.Y. Combined mesh free method and mode matching approach for transmission loss predictions of expansion chamber silencers. *Eng. Anal. Bound. Elem.* **2017**, *84*, 168–177. [CrossRef]
37. Gabard, G.; Astley, R.J. A computational mode-matching approach for sound propagation in three-dimensional ducts with flow. *J. Sound Vib.* **2008**, *315*, 1103–1124. [CrossRef]
38. Cummings, A.; Chang, I.J. Sound attenuation of a finite length dissipative flow duct silencer with internal mean flow in the absorbent. *J. Sound Vib.* **1988**, *127*, 1–17. [CrossRef]
39. Kirby, R. Simplified techniques for predicting the transmission loss of a circular dissipative silencer. *J. Sound Vib.* **2001**, *243*, 403–426. [CrossRef]
40. Panneton, R. Modelisation Numerique Tridimensionnelle par Elements Finis des Milieu Poroelastiques: Application au Probleme Couple Elasto-Poro-Acoustique. Ph.D. Thesis, Université de Sherbrooke, Sherbrooke, QC, Canada, 1997.
41. Jiang, C.; Wang, C.; Huang, L. Acoustic characterization of ducts lined with poroelastic materials based on wave finite element method. *Appl. Acoust.* **2019**, *145*, 362–373. [CrossRef]